The Use of Spaceborne Radar Data to Model Inundation Patterns and Trace Gas Emissions in the Central Amazon Floodplain

Åke Rosenqvist

Joint Research Centre of the EC, Space Applications Institute, GVM Unit, I-21020 Ispra, VA, Italy

Bruce R. Forsberg and Tania Pimentel

National Institute for Amazonian Research, INPA-CPEC, C.P. 478, Manaus, AM, Brazil 69011-970

Yrjö A. Rauste

VTT Automation, Remote Sensing, Box 13002, 02044 VTT, Finland

Jeffrey E. Richey

University of Washington, School of Oceanography, Box 357940, Seattle, WA 98195-7940, USA

ABSTRACT

River floodplains are the dominant wetland habitat in the Amazon river basin. They provide important habitat for aquatic flora and fauna and play a key role in sustaining regional fish production (Junk 1997; Forsberg *et al.* 1993). River floodplains are furthermore globally significant sources of methane (CH_4) and other trace gases essential to climate regulation (Devol *et al.* 1988). Refined information on wetland distributions and dynamics are currently needed to improve estimates of habitat availability and to calculate regional contributions of trace gases, especially CH_4, to the troposphere.

This paper describes how multi-temporal time series of spaceborne L-band SAR data from the Japanese Earth Resource Satellite 1 (JERS-1) were used to generate a model of the spatial and temporal variation of inundation on the floodplain of a typical black water river in the Central Brazilian Amazon and how this model was utilized, together with *in situ* measurements of river stage heights and methane (CH_4) fluxes, to improve regional estimates of CH_4 emissions.

We also demonstrate how a JERS-1 SAR time series can be used to map the spatial variation of flood duration on the Jaú river floodplain, a key factor controlling local variations in plant biodiversity

For both applications, the availability of adequate time series of satellite data proved to be a crucial factor affecting the reliability and accuracy of the flood models and the spatial details of the flood duration map. The availability of in-situ data, especially daily river height measurements, was also critical for the development of the flooding model and for the subsequent de-coupling of this model from the satellite data.

1. BACKGROUND

1.1 Target characteristics

The Jaú river is a black water tributary to the Negro river, located about 200 km upstream from the city of Manaus, in the central Amazon basin [figure 1]. It stretches 260 km from its headwaters to the confluence with the Negro and drains an area of about 17,000 km^2 dominated by lowland (terra firme) rain forest and seasonally inundated *igapó* floodplain forest.

Figure 1. *Extract from the GRFM mosaic (May-June 1996). Central Amazon Basin and the Jaú river drainage basin. The white box indicates the location of the field site (figure 2).*

JERS-1 GRFM © NASDA/MITI/JPL

The Jaú basin is the largest national park in Brazil and an important field site for ecological research. It is also a focal point for studies of floodplains as regional sources of tropospheric CH_4. The National Institute for Amazonian Research (INPA) and the non-governmental Fundação Victora Amazônica maintain a floating research laboratory in the river, approximately 50 km upstream the main channel, as well as a permanent gauging station where daily river stage measurements have been recorded since mid 1993.

The timing, duration and spatial extent of seasonal flooding events in the Jaú are parameters that affect both local ecology and regional CH_4 fluxes, and they are known to vary within the basin. Information about the former two parameters has been limited to a few point measurements along the river, while information on the spatial extent of flooding and its variations over time have been generally unavailable due to the lack of suitable measurement techniques. While optical remote sensing

data can be used to delineate the thematic extent of the *igapó* floodplain, it can not be used to map the (instantaneous) *extent of inundation*, key parameter in the context of this investigation, since flooding mainly occurs beneath the evergreen canopy layer.

However, while traditional optical instruments cannot be used, Synthetic Aperture Radar is known to be sensitive to this feature (e.g. Hess *et al.* 1995). Given a sufficiently long wavelength (L-band [23.5 cm], or longer), the microwave signal will penetrate the forest canopy and interact with structures further down in the forest, such as branches and trunks, and the ground. A like-polarized L-band signal - such as the L_{HH} signal of the JERS-1 SAR - is particularly sensitive to vertical structures on a horizontal surface, under certain circumstances producing a dihedral trunk-ground - or ground-trunk - reflection back towards the sensor. The magnitude of the backscattered signal depends to a large extent on the ground media, which is the key parameter to detecting forest inundation by SAR. While a non-flooded forest floor, due to its soil roughness and di-electrical properties, usually causes diffuse and lossy scattering, the smooth water surface of a flooded forest floor provides optimal conditions for non-lossy scattering. The diffuse ground interaction is, in the latter case, thus traded for a specular trunk-water (or water-trunk) reflection, which results in a significantly stronger backscatter. Figure 1 shows a part of a JERS-1 L-band SAR mosaic, covering the central part of the Amazon basin during the high water season in May-June 1996. Flooded forest areas appear bright in the imagery.

Figure 2. *Jaú river. Location of verification transect and gauge station. Full resolution JERS-1 SAR data (12.5 m pixel spacing). GRFM © NASDA/MITI*

1.2 Satellite and field data

With the objective of investigating the spatio-temporal dynamics of flooding events in the Jaú, JERS-1 SAR data were acquired regularly over the basin within the framework of the Global Rain Forest Mapping (GRFM) project, mainly between September 1995 and August 1997. These dedicated acquisitions resulted in seven full and two partial coverages over the entire basin (JERS passes 417-421), as well as 15 consecutive (44-day interval) observations over the part of the basin where the floating lab and the gauge station are located (pass 418). The first part of this paper will be focused on the latter smaller area, which has been used as a test region for the development of the spatio-temporal flooding model.

For in-situ verification of flooding extent and measurements of CH_4 fluxes, a 2.7 km long transect was opened through the seasonally flooded igapó forest, approximately 6 km downstream from the gauge station (figure 2). The transect begins at the rivers edge and ends in the (permanently dry) terra firme forest, covering a broad range of flooding conditions. Ten collection points were established along this transect at 300 meters intervals and sampled every six weeks during 1996 and 1997, in approximate synchrony with the satellite acquisitions. Measurements of water depth and CH_4 emissions were made at each point. Methodologies used for measurements and analysis of the CH_4 fluxes are described further in section 3. Figure 3 shows the annual variations in river stage measured in the Jaú, and the timing of the satellite acquisitions and field campaigns.

Figure 3. *River levels in Jaú river and corresponding JERS-1 acquisitions (❍) and field measurements (▲).*

2. Spatio-temporal modeling of seasonal inundation patterns

2.1 Work approach

The development of the spatio-temporal inundation model in the Jaú river basin, and its subsequent linkage to a CH_4 flux model, can be divided into the following major steps:

- Characterization of the radar backscatter properties of flooded/non-flooded forest;
- Estimation of flooded area for each date in the multi-temporal image sequence;
- Establishment of an analytical relationship linking flooded area to river stage;
- Estimation of the daily extent of flooding using the analytical relationship and daily stage data;
- Establishment of analytical relationships linking CH_4 flux to river stage and flooded area.
- Estimations of daily CH_4 fluxes from the whole Jaú river basin.

2.2 Radar backscatter characteristics

For a regional scale study of flooding patterns and CH_4 fluxes such as this, a spatial resolution of 100 metres is considered a fair trade-off between data amounts and spatial details. The full resolution SAR data were thus reduced from 12.5 to 100 metres pixel spacing by wavelet decomposition, thereby also decreasing speckle noise to reasonable levels of some 200 independent looks per pixel.

Table I shows the radar backscatter characteristics along the verification transect in the Jaú basin at seven different time points, between March 1996 and April 1997. Each value represents the radar backscatter for one 100 m pixel, expressed in linear digital number (DN). Dark grey (shaded) values indicate pixels verified in the field as flooded, while white values (non-shaded) were verified as dry. The limit of flooding along the transect was verified with 300 metres intervals, leaving a zone of at least 3 pixels around the flooded/non-flooded interface as unconfirmed. These pixels, plus an additional buffer of 1-2 pixels (light grey shaded figures within brackets) were considered uncertain, or mixed, and were therefore excluded from the analysis.

Although not included in table I, pixels immediately on the left and right hand side of each of the transect pixels were accounted for in computations, in order to obtain a larger number of samples. The flooding condition for those pixels were assumed to be the same as that of their corresponding centre pixel. For statistical description of the permanently dry terra firme forest, a number of pixels in the terra firme were added to the analysis.

The statistical characteristics of flooded igapó, non-flooded igapó and terra firme forest are given in table II. The means of the flooded and non-flooded igapó differed significantly, by almost 2.5 dB when expressed in logarithmic terms. Flooded igapó also showed a wider spread in the data. The distributions of terra firme and non-flooded igapó were however very similar, both in terms of mean and in variance, and the two classes were therefore treated as a single, non-flooded, class, referred to in the analysis below as "dry forest".

Table I. *Temporal variations in L-band backscatter (linear DN) along the Jaú transect. Shaded and white boxes indicate in-situ verified flooded resp. dry points. Figures within brackets indicate points with unverified or mixed flooding conditions.*

Table II. *L-band backscatter statistics (linear DN) of in-situ verified points along the transect.*

2.3 Estimation of flooded area

2.3.1 Model development

With the distributions of flooded and dry forest characterized, the next step was to count the number of flooded pixels in order to estimate the flooded area. A certain overlap however existed between the two classes and in order to be able to correctly estimate the number of flooded pixels in the SAR imagery, this ambiguity between the classes had to be resolved.

Figure 4. *Backscatter distribution of (linear DN) of flooded and dry transect points.*

Figure 4 illustrates the distributions of flooded and dry forest as measured along the verification transect in the multi-temporal image sequence. By applying an arbitrary threshold to the data, it follows that a certain number of pixels from each class will be incorrectly classified. The numbers of misclassified pixels for each class for a given threshold are however not unknown, but given by the class distributions, thereby possible to quantify and correct for.

A'_F and A'_D in figure 4 indicate number of pixels (areas) classified as flooded resp. dry, for an arbitrary threshold value, while A_F and A_D represent the "true" numbers of flooded and dry pixels. ε_F and ε_D denote the fractions of misclassified pixels, which are functions of the threshold level. By masking out open water (black in the imagery), we can reduce the question to a two-class problem, where the total number of pixels in the area of interest, A_{TOT} , is simply the sum of the number of flooded and dry pixels:

$$A_{TOT} = A_F + A_D \; (= A'_F + A'_D) \qquad (1).$$

The number of pixels classified as flooded forest can be expressed as:

$$A'_F = A_F - (A_F \, \varepsilon_F) + (A_D \, \varepsilon_D) \qquad (2)$$

and by substituting A_D for $(A_{TOT} - A_F)$ in equation (2), the "true" number of flooded pixels is given by:

$$A_F = (A'_F - A_{TOT}\,\varepsilon_D)\,(1 - \varepsilon_F - \varepsilon_D)^{-1} \qquad (3).$$

For a given area of interest, e.g. a sub-region in the river basin, only A_F remains unknown in equation (3), while A_{TOT} is fixed, and A'_F, ε_F and ε_D are given by the threshold value. Hence, the "true" number of flooded pixels can be calculated. Furthermore, provided that the statistical distributions of flooded and dry forest are correctly characterized, the value of A_F should be the same for *any* threshold value.

Table III. *Flood area estimates in Jaú river (basin 3) before and after correction of misclassified pixels. The correction coefficients (ε_x) indicate the fractions of misclassified pixels for a given threshold value prior to correction.*

Table III shows the estimated flooding in a sub-section of the Jaú basin on seven different occasions between October 1995 and November 1996. The left hand side of the table shows the threshold values used and the resulting area estimations (A'_F), before correction by equation (3). For a given date, the value of A'_F consequently decreased as the image threshold slided from low towards higher pixel values. The right hand side of the table, on the other hand, shows the flood estimations after correction of misclassified pixels, as well as the corresponding correction coefficients (ε_F and ε_D) used. The area estimates for each of the seven dates were quite consistent and tended to converge around a single value, with a standard deviation of around 2-4 km^2.

2.3.2 Error sources

The performance of the above correction procedure depends on several factors. Most important is perhaps the characterization accuracy of the reference backscatter distributions of the flooded and dry forest classes. Ground verification is, in this context, essential. It is also clear that a large number of in-situ samples will improve the reliability of the reference distributions. The 540 points sampled along the Jaú transect provided a fair description, but with increasing uncertainties for the very high and low values where the distributions trail off.

It is also acknowledged that the procedure does not take into account mixed pixels, e.g. along the river/igapó contact, or along the flooded/non-flooded interface. The exact location of the flooding along the verification transect could not be determined with such precision (hence the excluded pixels in table I) and a mixed class could thus not be characterized. The misclassification resulting from this flaw is however considered to be small, except in areas with a limited amount of flooding. It is furthermore

not expected to introduce any bias into the flood estimation, as the misclassifications in favour of one class or the other can be assumed to be randomly distributed.

Another issue is the ecological representativity of the sample area in terms of the vegetation distribution in the entire study area. In our case, the transect is known to represent a typical cross section of the vegetation types found in the Jaú floodplain, and in black water floodplains in general. For application of the methodology to other parts of the Amazon basin, though, for example to the white water tributaries along the Solimões river, the validity of the reference distributions along the Jaú transect would have to be confirmed, and possibly re-defined.

The performance of the procedure also depends on the relative (scene-to-scene) calibration accuracy of the satellite data, which for JERS-1 SAR is in the order of about 1 dB (Shimada 1996). A radiometrical deviation in the data, in relation to the radiometry of the transect scenes used, will inevitably result in an over- or under estimation of the flooded area. Shimada and Freeman (1995) have however shown that [terra firme] rain forest may be used as a distributed reference target for radiometric calibration, and individual correction of the scenes used in this study would thus in principle be possible. However, with some 70 scenes at hand for the time series over the entire Jaú basin, this approach was deemed impractical. An alternative way to approach this problem is to adjust for offset radiometry simultaneously with the flood estimation, as an additional artefact of deviating radiometry is that the flooded area estimates (A_F) do not converge towards a specific value. This effect can be used as an indicator of radiometric inconsistency, which can be adjusted for by introducing a corresponding radiometric shift to the values of the reference class distributions. The magnitude of this "correction shift" varies from scene to scene, and even within scenes, and is fixed to the value where the area estimates (A_F) again converge properly.

Figure 5 (a - c). *Seasonal inundation in the Jaú river basin. GRFM © NASDA/MITI*

Figure 5 (d - e). *Seasonal inundation in the Jaú river basin. GRFM © NASDA/MITI*

2.3.3 Basin-wide inundation modeling

In order to estimate the flooding dynamics in the entire Jaú basin, nine basin-wide mosaics were compiled from the JERS-1 time series. The mosaicking procedures utilized were those developed within the GRFM project by the JRC for the African continent, as described by Rauste *et al.* (1999a, 1999b). Figure 5 (a-e) shows a part of the mosaic sequence, from the 1995-1996 flood cycle.

The Jaú basin was divided into 17 sub-regions (figure 5 (a)) to obtain better correlation with the gauge measurements, which were limited to single one point along the river (near the transect in sub-basin 3). The sub-regions were delineated to, as far as possible, correspond to local independent drainage basins, or parts thereof. The availability, or non-availability, of satellite data also influenced the definition. It is important to notice, in this context, that five adjacent JERS-1 passes were required to cover the basin, thereby introducing a temporal off-set within the mosaics. As the JERS-1 satellite acquired data in a systematic, east-to-west, manner, with adjacent swaths being observed on consecutive days, this resulted in a 1-day time difference between each of the passes, so that the Jaú headwaters in the west were always acquired five days after that of the Jab-Negro confluence in the east.

Beginning with the sub-basin where the verification transect and the gauge station were located (basin 3), the estimated flooded area was plotted against the corresponding river stage height for all JERS-1 data takes available over that particular pass (Fig. 6a). As expected, there was a strong correlation between flooded area and river stage ($r^2 = 0.97$), and an analytical relationship was easily established. The same was true for the two sub-basins further downstream, whose flood dynamics were also closely correlated ($r^2 > 0.92$) with basin-3 stage variations.

For basins located upstream (basins 4-11), on the other hand, the flood peak was out of phase with the stage peak at the gauging station. In the Jaú headwaters, for instance (sub-basin 11), the peak of flooding normally occurs around March - several months before basin 3 reaches its maximum in June-July. This introduces a discontinuity in the correlation between flood extent and the gauge data, which is present for all the upstream sub-basins. In these cases, the relationships had to be divided into two or more functions that were valid only within certain intervals, typically depending on whether the basin-3 stages were rising or falling (figure 6 (b)).

The flooding in the Carbinani tributary was more difficult to relate to the Jaú stage data since its confluence with the Jaú main channel is located considerably downstream of the gauging station. Water levels in the Carbinani thus are not be expected to be correlated to those in the Jaú upstream of the confluence. Although figure 6 (c) suggests a weak relationship with the Jaú river stage, it is presumably and an indirect one, reflecting similar responses to regional precipitation patterns. The same is valid for the interfluvial wetlands located between the two rivers, shown in figure 6 (d). This swampy area is particularly sensitive to local precipitation events and drains primarily into the Carbinani.

The establishment of more gauging stations along the Jaú and Carbinani main channels would clearly provide better and more accurate relationships, but this has, for logistical reasons, not been feasible. Nevertheless, the relationships established here for the Jaú main channel are considered reasonable. Although somewhat coarse in the upper part of the basin, they still represent the best models available for describing the flooding patterns along the Jaú.

With the relationships described above, the flooded area along the Jaú may now be predicted on a daily basis, using stage measurements as input. Flooding extent may be estimated continuously from 1993, when the gauge station was established, to the present date, with no further image analysis. The flooding model has, in other words, been de-coupled from the satellite data.

Figure 6 (a-d). *River stage height vs. flooded area for four sub-basins in the Jaú river basin (O - rising stages; X - falling stages). Analytical relationships between river stage and flooded area could only be obtained for sub-basins along the Jaú main channel (1-11)*

Figure 7. *Variations in flooded area during the 95/95 and 96/97 flood cycles. Area estimates in the Jaú river (basins 1-11) derived analytically from daily gauge records. Estimates for the Carbinani river and the interfluvial area derived by linear interpolation between estimates in JERS-1 SAR data.*

In the Carbinani and the interfluvial areas, however, correlation with river gauges measured in the Jaú main channel were not considered acceptable for the establishment of analytical relationships. Flood modeling in these areas has therefore been limited to the 1995-1996 flood cycle, where daily flood extents have been obtained through linear interpolation between area estimations made in the JERS-1 time series, depicted in figure 5 above.

Figure 7 shows the daily flooding extents in the Jaú main channel (sub-basins 1-11) in the period 1993 – 1998, estimated as the sum of the flooded areas calculated from the analytical relationships established for the different sub-basins. Area estimates derived from SAR imagery (indicated with X) show good correspondence with the analytical curve.

3. CH_4 EMISSION MODELING

3.1 CH_4 flux measurements

Four replicate estimates of methane emissions were made at each point along the transect during each sampling campaign using static chambers. The chambers and methods used are similar to those described by Devol *et al.* (1988) and Pulliam (1993). Under flooded conditions a floating chamber was used, consisting of a polyethylene cylinder, open at the bottom and covered with styrofoam, except for a 2 cm polyethylene lip which protruded at the bottom. The styrofoam held the chamber in a fixed position while floating, maintaining a constant internal volume. A terrestrial chamber was used when the forest floor was dry, consisting of an aluminium cylinder with a removable cover and an open bottom with a bevelled edge. When this chamber was deployed the bevelled edge penetrated the forest floor to a depth of approximately 1 cm to limit atmospheric exchange. The cover was removed initially so that the internal dimensions of the cylinder could be determined and then closed during the measurement. In both cases (floating and terrestrial chambers), the chambers were deployed for a period of 20 minutes, during which gas samples were withdrawn a regular intervals with 60 ml polyethylene syringes fitted with gas-tight valves. Samples of ambient air and surface water were also collected with 60 ml syringes. Water samples were equilibrated in the sampling syringe with an equal volume of ambient air which was analyzed to determine the concentration of methane in the water. All gas samples were immediately transferred to serum vials with gas-tight butyl rubber stoppers and stored in the dark for 1 –10 days before analysis. CH_4 concentrations were determined by gas chromatography using a Perkin Elmer chromatograph fitted with an FID detector and a Porpac-N column. Areal methane emission rates (mg C m^{-2} d^{-1}) were estimated from the change in CH_4 concentrations in the chamber during incubation, accounting for chamber volume and area. Significant methane emissions were encountered primarily under flooded conditions (table IV). Fluxes on dry land were either slightly

negative or slightly positive and generally low. We will therefore focus our discussion on the flux dynamics under flooded conditions.

Table IV. *Temporal variations in CH_4 flux [mgC/m^2/day] along the 10 transect points.* ***Shaded boxes*** *indicate inundated points.*

The spatial and temporal pattern of methane emissions was closely tied to the annual flooding pattern. Significant emissions occurred initially during the rising water period near the river margin, moving gradually inward toward the terra firme margin as the river level rose. The reverse trend was observed during the falling water period. The fluxes during falling water were significantly higher than those observed during rising water, reflecting the gradual build-up of CH_4 in the water column during the flooded period. The higher falling water fluxes also reflect the effects of reduced hydrostatic pressure on the emission of bubbles. This effect will be discussed further in the following section. Significant differences were also observed between fluxes along the flooded transect on a given date, where fluxes often were significantly higher at the terrestrial-aquatic interface. This may reflect local disturbances of the bottom sediments at these shallow sites caused during the measurement procedure or a natural increase in biological activity at this dynamic transition zone (Junk et al. 1989). No consistent relationship was found, however, between methane flux and water column depth, and cross-transect differences were generally much smaller than the average difference observed for the whole transect between sampling dates.

Figure 8. *Empirical relationship linking methane fluxes to daily rate of change in river stage.*

3.2 Hydrostatic flux model

To extrapolate the flux results obtained from the transect to other dates and to other parts of the Jaú basin it was necessary to develop an empirical model linking the observed fluxes to parameters with greater spatial and temporal resolution. River stage height, an effective predictor of flooded area, proved to be useful in this case as well. A strong negative relationship was found between the estimated methane flux and the rate of change in stage height estimated for the 10 day period preceding the flux measurement (figure 8).

The rate of change in stage height has a direct effect on the level of hydrostatic pressure in the water column which, in turn, appears to have a strong effect on the rate of formation and release of methane bubbles. The chambers showed a major increase in total flux when the river level was falling rapidly, reflecting this effect. The empirical relationship developed between methane flux and stage change allowed us to predict the methane flux in the entire flooded area in sub-basin 3 on a daily basis, by use of the daily gauge data. The same relationship could be extrapolated to basin 4 and the two basins downstream of the transect (basins 1 and 2).

The basin 3 stage records were however not considered representative for the stage fluctuations in areas upstream of the gauge station (sub-basins 5-11), along the Carbinani or in the interfluvial region (basins 12-17). The rate of change in flooded area for each sub-basin, normalized by its maximum extent of flooding, was instead developed as a proxy parameter in these areas.

4. Regional flux estimations

With CH_4 emissions expressed as functions of [rate of change in] river stage, in units of [flux area^{-1}day^{-1}], regional flux estimates for the Jaú basin could be obtained by coupling the flux relationship with the daily estimations of flooding extent, also expressed as functions of river stage. Figure 9 (a) shows the estimated monthly fluxes from the Jaú main channel (basins 1-11) during five flood cycles between 1993 and 1998. As both the flux and the flooding models had river stage height as the only input parameter, fluxes could be estimated as far back in time as the gauge data permitted (July 1993), i.e. long before the site was targeted by JERS-1 acquisitions or subject to CH_4 in-situ measurements. Fluxes may also be estimated in real-time on a daily basis as far into the future as the gauge station remains in operation.

Figure 9a. *Estimated monthly CH_4 emissions (10^3 kg of C month^{-1}) from the Jaú river (basins 1-11) 1993-1998. Accumulated annual estimates are given for each flooding cycle.*

The model results indicate that emissions are generally low during the first few months of rising water levels, gradually increasing in the period February-March and onward as the stages in the Jaú headwaters begin to fall. The fluxes peak in May through August, emitting an estimated 1500 - 2500 tons of carbon monthly during this period of time. The accumulated

annual fluxes for each of the five flooding cycles vary around 10,000 tons per year for this part of the basin (sub-basins 1-11), except during the El Niño year 1997/1998, where the estimated emissions dropped to less than 7500 tons.

Figure 9 (b) shows the total estimated accumulated CH_4 emissions during the flood cycle of 1995/1996, including data for the Carbinani tributary and the interfluvial region, whose flooded areas and proxy stage change estimates - due to poor relationships with the Jaú gauges - were retrieved through linear interpolation between JERS-1 derived flood estimates (figure 7) solely for this flooding cycle. The graph indicates a total flux of some 17,000 tons of carbon from the entire Jaú drainage basin during this particular year, with the contribution from each of the three areas in relative proportion to their respective domain.

Figure 9b. *Accumulated monthly CH_4 emissions during the 1995/1996 flooding cycle for the entire Jaú river basin. Flood estimates in for the Carbinani and interfluvial area obtained through linear interpolation between JERS-1 derived area estimates.*

5. FLOOD DURATION MAPPING

5.1 Floodplain biodiversity

Apart from being natural sources of tropospheric CH_4, the alluvial floodplains sustain rich and diverse ecosystems. The annual inundation pulse has been identified as the dominant environmental factor affecting aquatic biota on the Central Amazon floodplain (Junk 1997) and, as has been illustrated above, the characteristics of this pulse, in terms of duration, extent, amplitude etc., varies spatially on the floodplain, as a function of fluctuations in river stage height and topography. This variation has been shown to control the distribution of floodplain fauna (Adis 1997) and flora (Junk and Piedade 1997).

Given the historical lack of appropriate techniques to study forest inundation, the availability of a spaceborne L-band SAR instrument provides a unique potential for mapping and monitoring the largely unknown spatial variations of flooding in tropical wetlands.

5.2 Flood mapping

For mapping of flood duration, the river basin has to be stratified into areas with equal or similar duration of flooding, and an essential criteria in this context is thus the availability of appropriate time series of SAR data. In order to avoid uncertainties caused by inter-annual variations in precipitation and river levels, it is strongly preferred that the satellite data be acquired during one single flood cycle. For the Jaú basin, time series of images were acquired from October to October. The annual sequence of images was especially important in basins like the Carbinani where no gauge data are available.

Flood duration maps were generated by thresholding the SAR data at a level corresponding to 5% misclassification ($\varepsilon_F = \varepsilon_D = 0.05$) of each of the two classes, followed by a 3x3 median filtering to remove solitary pixels (typically isolated flooded pixels in the terra firme forest). To compensate for the regional scale radiometric variances within the mosaics, the thresholding procedure was performed separately for each of the 17 sub-basins by taking the corresponding radiometric off-set into account.

Figure 10 shows the spatio-temporal dynamics of flooding in the Jaú river basin during the 1995/1996 flood cycle. This map - at 100 metres pixel spacing in its original form - constitutes the first information available about the spatial characteristics of a regional scale annual inundation phenomena. The map indicates, for instance, that the lower one third of the Jaú main channel is exposed to the longest periods of inundation in the basin. It also indicates a similarity between the upper part of the Jaú river and the Carbinani tributary, which both are subject to significantly shorter periods of flooding. These similarities in flood duration may e.g. indicate similarities in tree species composition and floodplain habitat distribution (Ferreira and Stohlgren 1999).

While unique, the map shown in figure 10 is nevertheless imprecise in its determination of the flooding periods. This is a result of the SAR data availability, which has a direct impact on the temporal resolution of the map. The complete Jaú basin was covered five times out of nine possible during the 1995/1996 flood cycle, which resulted in several holes in the temporal sequence (Table V).

Table V. *JERS-1 SAR data availability over the Jaú river drainage basin (paths 417-421) and the verification transect (path 418), respectively, during the 1995/1996 flood cycle.*

Figure 10. *Flood duration in the Jaú river drainage basin, extracted from JERS-1 SAR time sequence of 5 data takes during the 1995-1996 flood cycle. Original pixel spacing 100 metres. GRFM © NASDA/MITI/JRC*

The path covering the transect (path 418) however, was acquired at every overpass during the 1995/1996 flood cycle, resulting in 9 consecutive acquisitions. Figure 11 shows a flood duration map derived from this complete time series of JERS-1 data, yielding a temporal resolution of 44 days (the JERS-1 repeat cycle). Along the Jaú main channel, where gauge measurements are available, the flood duration map also reveals the local ground topography in the area, where each colour level represents a topographic equidistance of about 1.5 metres (see figure 3 above). Due to the lack of additional gauge stations, this analysis cannot however be extended to the Carbinani river or the interfluvial area.

Figure 11. *The Jaú and Carbinani rivers, and the rain fed interfluvial area (JERS path 418). Flood duration map extracted from JERS-1 SAR time sequence of 9 consecutive data takes. Temporal resolution 44 days. GRFM © NASDA/MITI*

6. CONCLUSIONS

The current study has demonstrated the usefulness of spaceborne L-band SAR for mapping and monitoring of the spatio-temporal dynamics of seasonal inundation events in tropical wetland areas. Apart from the long L-band wavelength, required to penetrate the forest canopy to detect standing water beneath, the capacity of performing repetitive measurements during the course of the flooding phenomena has proved to be essential. For mapping of the spatial and temporal extent of flooding, data acquisitions are required during one and the same flood cycle, preferably during each overpass of the satellite within that period of time.

The study has also shown that L-band SAR time series can be used to estimate flooding extent on a daily basis, by linking area estimations of flooding in the SAR data to daily in-situ measurements of river stages. Through regression analysis, estimations of flood extent have been de-coupled from the satellite data, and expressed solely as functions of river stage. The

availability of gauge stations along the relevant river channels are, in this context, fundamental, as stage-area relationships can only be established satisfactory in areas with representative stage readings.

The analytical flooding model developed here has been used as input for estimations of regional CH_4 emissions from the Jaú river basin, where daily CH_4 fluxes were derived as functions of flooded area and rate of change in river stage. Minimum fluxes in the basin were recorded annually October through December during rising water levels, while the emissions peaked during the falling gauges between May and August. With about 10% of the Jaú river basin (~1,700 km^2) consisting of seasonally inundated igapó forest, the accumulated CH_4 fluxes for the entire basin were estimated to be 17,000 tons of carbon per year.

Extrapolation the current models to the entire Amazon river basin, both for flood duration mapping and for CH_4 estimations, will be attempted by use of the basin-wide mosaics generated over the Amazon within the GRFM project, featuring the basin at two occasions in time (October-November 1995 and May-July 1996). Based on the findings in this study however, it is clear that the temporal resolution possible to achieve will only suffice for coarse stratifications of flood duration and estimations of trace gas fluxes.

It is thus recognized that the technical tools and methodologies for improving continental scale estimates of CH_4 emissions - which presently are a significant source of uncertainty in global green house gas models - do exist, but cannot be fully explored due to the lack of adequate time series of satellite data. It is therefore recommended that the next generation of L-band SAR satellites - in particular the ALOS satellite which is due for launch in 2002 - be subject to a data acquisition strategy dedicated to collection of consistent time series of data. This should comprise monthly, or bi-monthly, acquisitions over global wetland areas during at least one full year.

With flood duration inherently linked to aquatic biodiversity, such a dedicated data acquisition strategy would constitute a significant leap forward in providing tangible information in the service of the global change research community, in line with the information requirements posed by relevant international treaties, such as the UN Framework Convention for Climate Change and the Convention on Biological Diversity.

Anthropogenic sources of CH_4, such as irrigated rice, acquaculture and hydro-electrical reservoirs can to a large extent be mapped by the same basic methodology, also with shorter wavelength SAR systems, and the request for the establishment of timely and spatially consistent data archives may thus be extended to comprise also C-band SAR systems such as e.g. ENVISAT.

7. ACKNOWLEDGEMENTS

This work was supported by NASDA, INPA, Fundação Vitória Amazônica, NASA and the Joint Research Centre. The JERS-1 data were provided by NASDA within the framework of the Global Rain Forest Mapping project.

REFERENCES

ADIS, J. 1997. Terrestrial invertebrates: Survival strategies, group spectrum, dominance and activity patterns. In Junk, W.J. [ed.] *The Central Amazon Floodplain*, Springer Verlag, Berlin. pp. 299-318.

DEVOL, A.H., RICHEY, J.E., CLARK, W.A. and KING, S.L., 1988. Methane emissions to the troposhpere from the Amazon floodplain. *Journal of Geophysical Research.* 93: 1583-1592

FERREIRA L.V. AND STOHLGREN T.J. "Effects of river level fluctuation on plant species richness, diversity, and distribution in a foodplain forest in Central Amazonia". *Oecologia*, 1999, 120:582-587.

FORSBERG, C. A. R. M. Araujo-Lima, L. A. Martinelli, R. L. Victoria and J. A. Bonassi. 1993. Autotrophic carbon sources for fish of the central Amazon. *Ecology* **74:** 643-652.

FORSBERG, B. R., HASHIMOTO, Y., ROSENQVIST, A., AND MIRANDA, F.P., Neotectonic control of wetland distributions in the central Amazon revealed by JERS-1 radar imagery. *Quaternary International* [in press]

HESS, L., MELACK, J., FILOSO, S., AND WANG, Y., 1995, Mapping wetland hydrology with synthetic aperture radar. *IEEE Transactions on Geoscience and Remote Sensing*, **33,** 896-904.

HESS, L., E. NOVO, D. VALERIANO, J. HOLT, AND J. MELACK, 1998. Large-scale vegetation features of the Amazon basin visible on the JERS-1 low-water Amazon mosaic. *Proceedings International Geoscience and Remote Sensing Symposium (IGARSS'98)*, Seattle, USA, 6-10 July 1998, Vol. II, pp. 843-846.

JUNK, W.J.,BAYLEY, P.B. AND R.E. SPARKS. 1989. The flood pulse concept in river-floodplain systems. In Dodge, D.P. [ed.] Proceedings of the International Large Rivers Symposium. Can. Spec. Publ. Fish. Aquat. Sci. 106.

JUNK, W.J. AND M.T.F. PIEDADE. 1997. Plant life in the floodplain with special reference to herbaceous plants. In Junk, W.J. [ed.] *The Central Amazon Floodplain*, Springer Verlag, Berlin. pp. 147-187.

JUNK, W.J. 1997. [ed.]. *The Central Amazon Floodplain: Ecology of a pulsing system.* Springer Verlag, Berlin, 525 p.

SHIMADA M., 1996. Radiometric and geometric calibration of JERS-1 SAR. *Advances in Space Research*, **17,** 79-88.

PULLIAM, W.M., 1993, Carbon dioxide and methane exports from a southeastern floodplain swamp. *Ecological Monographs*, **63,** 29-54.

ROSENQVIST, Å., FORSBERG, B.R., PIMENTEL, T. AND RICHEY, J.E., 1998, Using JERS-1 L-band SAR to Estimate Methane Emissions from the Jaú River Floodplain (Amazon/Brazil). *Proceedings International Geoscience and Remote Sensing Symposium (IGARSS'98)*. Seattle, USA, 6-10 July 1998. Vol III, pp 1623-1625. IEEE Catalog No. 98CH36174.

SHIMADA, M. AND FREEMAN, A., 1995, A Technique for Measurement of Spaceborne SAR Antenna Patterns Using Distributed Targets. *IEEE Transactions on Geoscience and Remote Sensing*, **33,** 100-114.

FIGURE CAPTIONS

Figure 1. Extract from the GRFM mosaic (May-June 1996). Central Amazon Basin and the Jaú river drainage basin. The white box indicates the location of the field site (figure 2). GRFM © NASDA/MITI/JPL

Figure 2. Jaú river. Location of verification transect and gauge station. Full resolution JERS-1 SAR data (12.5 m pixel spacing). GRFM © NASDA/MITI

Figure 3. River levels in Jaú river and corresponding JERS-1 acquisitions (❍) and field measurements (▲).

Figure 4. Backscatter distribution of (linear DN) of flooded and dry transect points.

Figure 5 (a - c). Seasonal inundation in the Jaú river basin,. GRFM © NASDA/MITI

Figure 5 (d - e). Seasonal inundation in the Jaú river basin,. GRFM © NASDA/MITI

Figure 6. River stage height vs. flooded area for four sub-basins in the Jaú river basin (O - rising stages; X - falling stages). Analytical relationships between river stage and flooded area could only be obtained for sub-basins along the Jaú main channel (1-11)

Figure 7. Variations in flooded area during the 95/95 and 96/97 flood cycles. Area estimates in the Jaú river (basins 1-11) derived analytically from daily gauge records. Estimates for the Carbinani river and the interfluvial area derived by linear interpolation between estimates in JERS-1 SAR data.

Figure 8. Empirical relationship linking methane fluxes to daily rate of change in river stage.

Figure 9a. Estimated monthly CH_4 emissions (10^3 kg of C $month^{-1}$) from the Jaú river (basins 1-11) 1993-1998. Accumulated annual estimates are given for each flooding cycle.

Figure 9b. Accumulated monthly CH_4 emissions during the 1995/1996 flooding cycle for the entire Jaú river basin. Flood estimates in for the Carbinani and interfluvial area obtained through linear interpolation between JERS-1 derived area estimates.

Figure 10. Flood duration in the Jaú river drainage basin, extracted from JERS-1 SAR time sequence of 5 data takes during the 1995-1996 flood cycle. Original pixel spacing 100 metres. GRFM © NASDA/MITI/JRC

Figure 11. The Jaú and Carbinani rivers, and the rain fed interfluvial area (JERS path 418). Flood duration map extracted from JERS-1 SAR time sequence of 9 consecutive data takes. Temporal resolution 44 days. GRFM © NASDA/MITI

TABLE CAPTIONS

Table I. Temporal variations in L-band backscatter (linear DN) along the Jaú transect. Shaded and white boxes indicate in-situ verified flooded resp. dry points. Figures within brackets indicate points with unverified or mixed flooding conditions.

Table II. L-band backscatter statistics (linear DN) of in-situ verified points along the transect.

Table III. Flood area estimates in Jaú river (basin 3) before and after correction of misclassified pixels. The correction coefficients (ε_x) indicate the fractions of misclassified pixels for a given threshold value prior to correction.

Table IV. Temporal variations in CH_4 flux [$mgC/m^2/day$] along the 10 transect points. **Shaded boxes** indicate inundated points.

Table V. JERS-1 SAR data availability over the Jaú river drainage basin (paths 417-421) and the verification transect (path 418), respectively, during the 1995/1996 flood

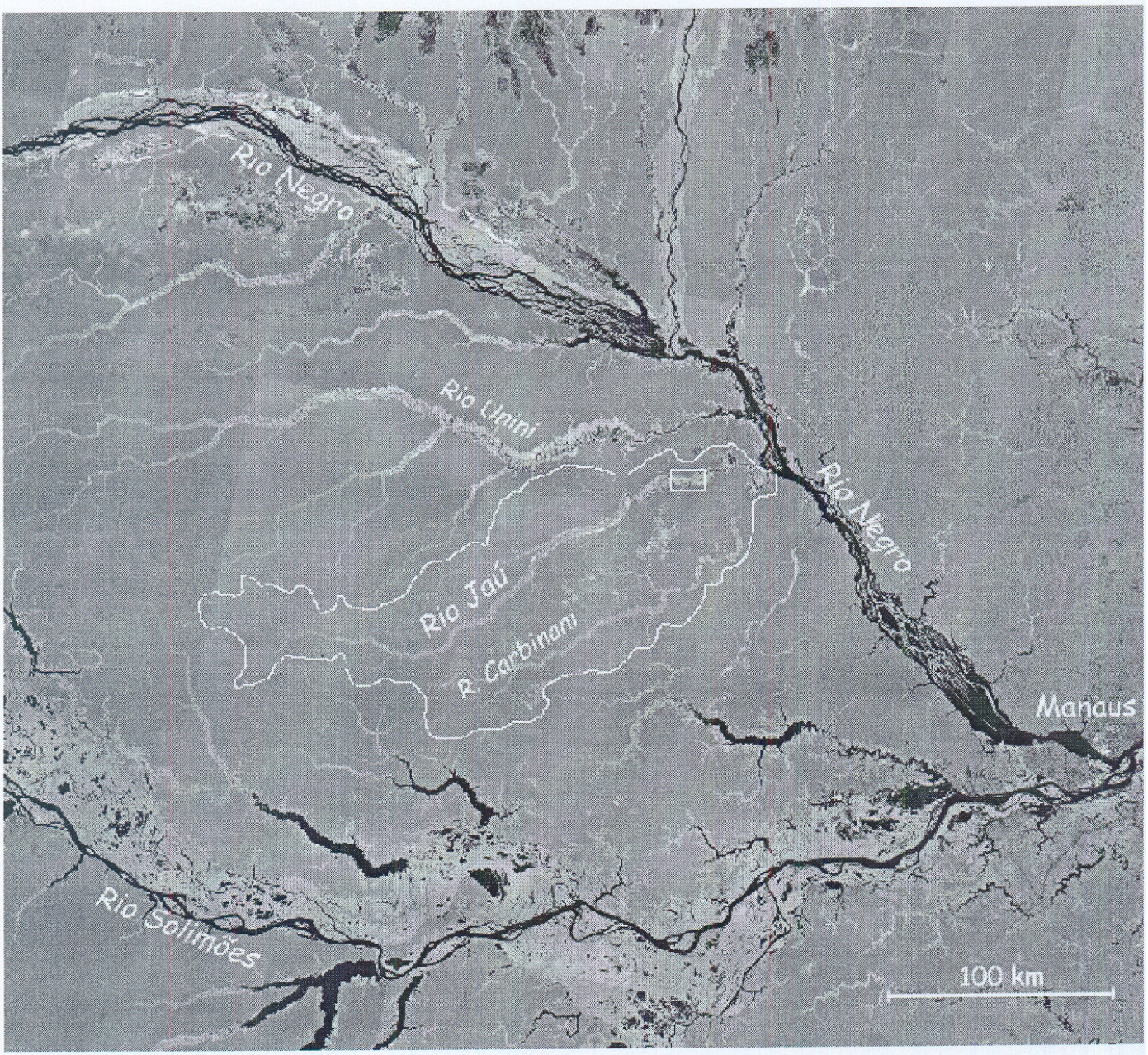

Figure 1. Extract from the GRFM mosaic (May-June 1996). Central Amazon Basin and the Jaú river drainage basin. The white box indicates the location of the field site (figure 2). GRFM © NASDA/MITI/JPL

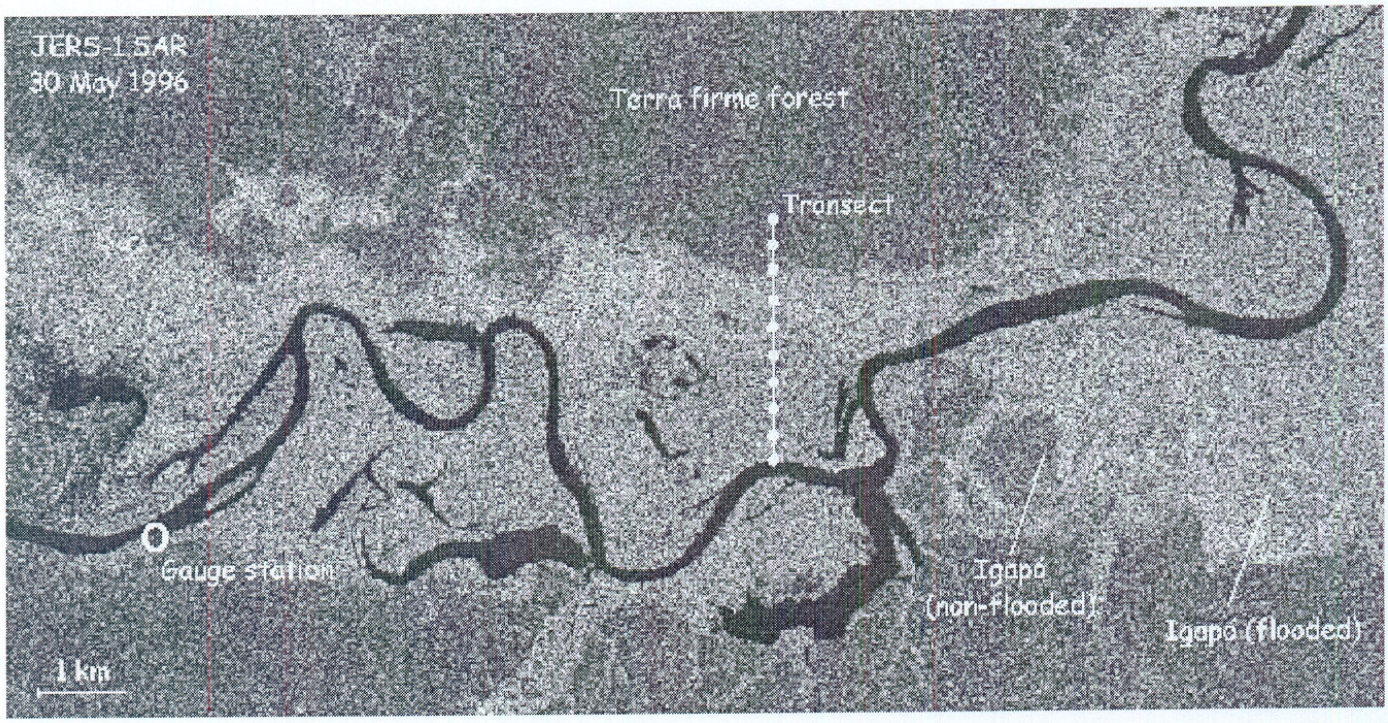

Figure 2. Jaú river. Location of verification transect and gauge station. Full resolution JERS-1 SAR data (12.5 m pixel spacing). GRFM © NASDA/MITI

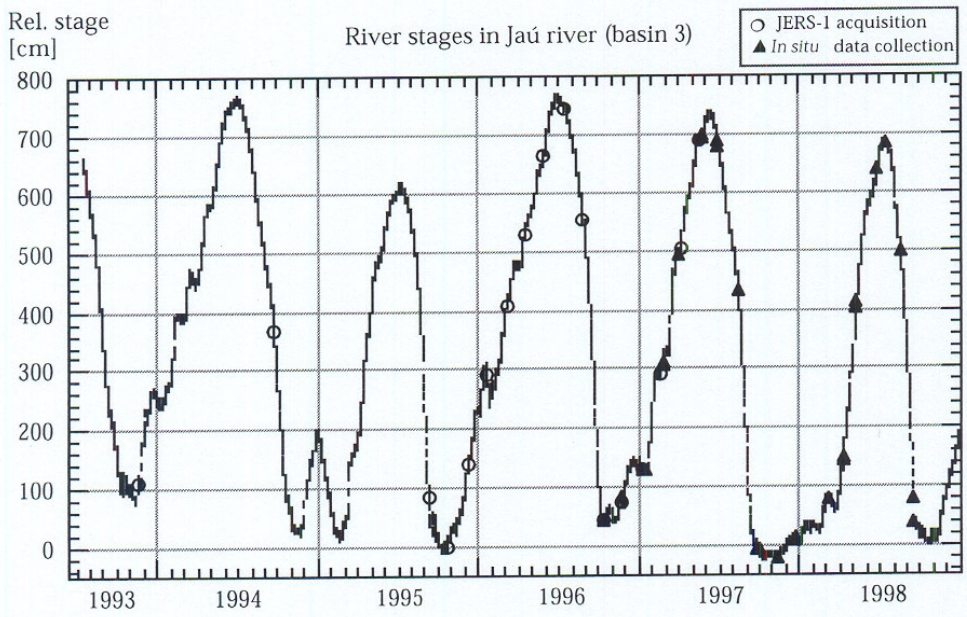

River levels in Jaú river and corresponding JERS-1 acquisitions (❍) and field measurements (▲).

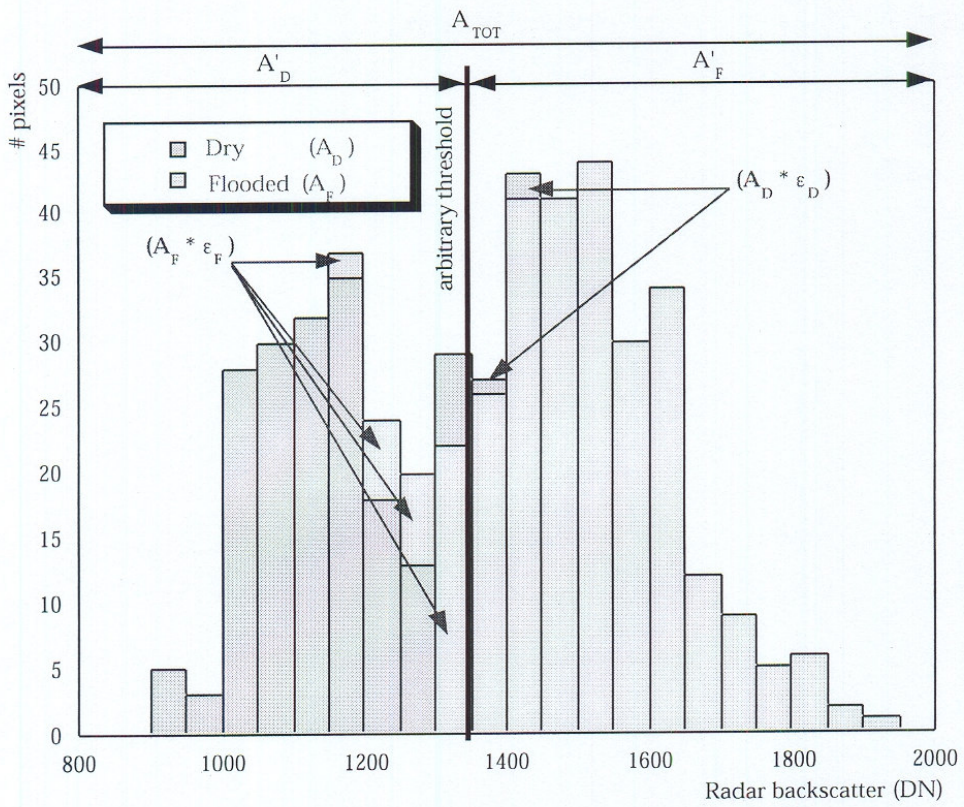

Figure 4. *Backscatter distribution of (linear DN) of flooded and dry transect points.*

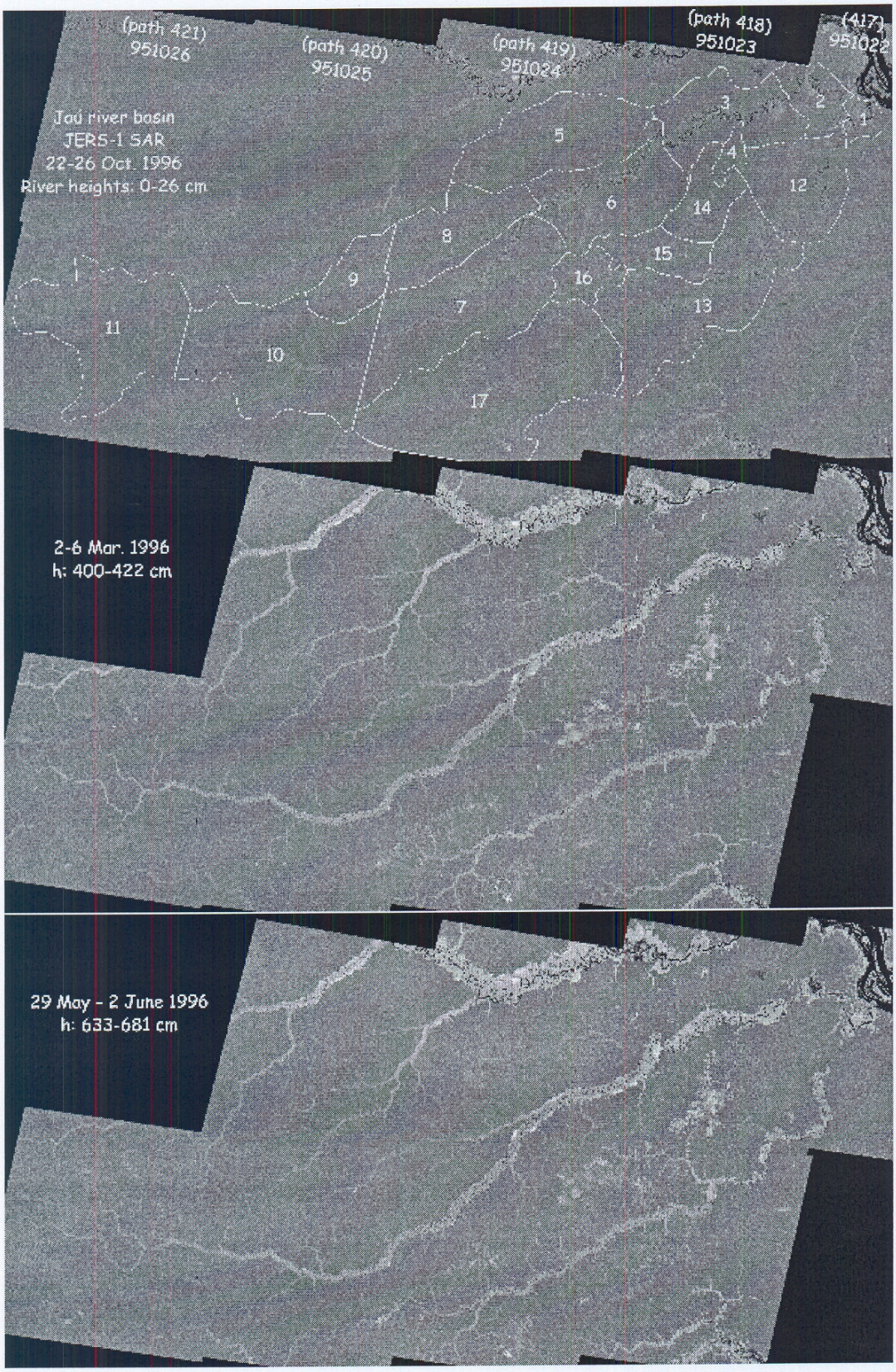

Figure 5 (a - c). Seasonal inundation in the Jaú river basin,. GRFM © NASDA/MITI

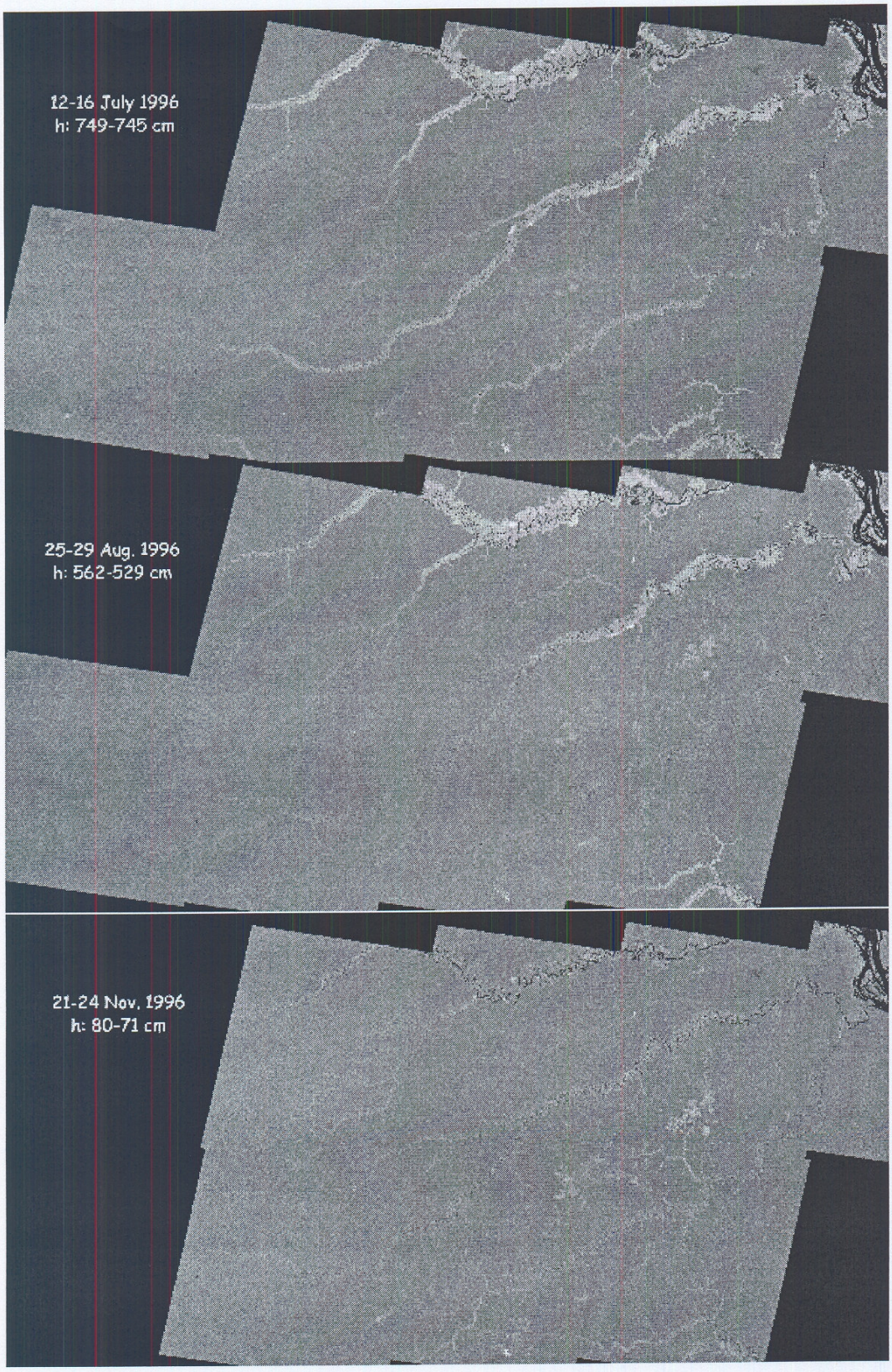

Figure 5 (d - e). Seasonal inundation in the Jaú river basin,. GRFM © NASDA/MITI

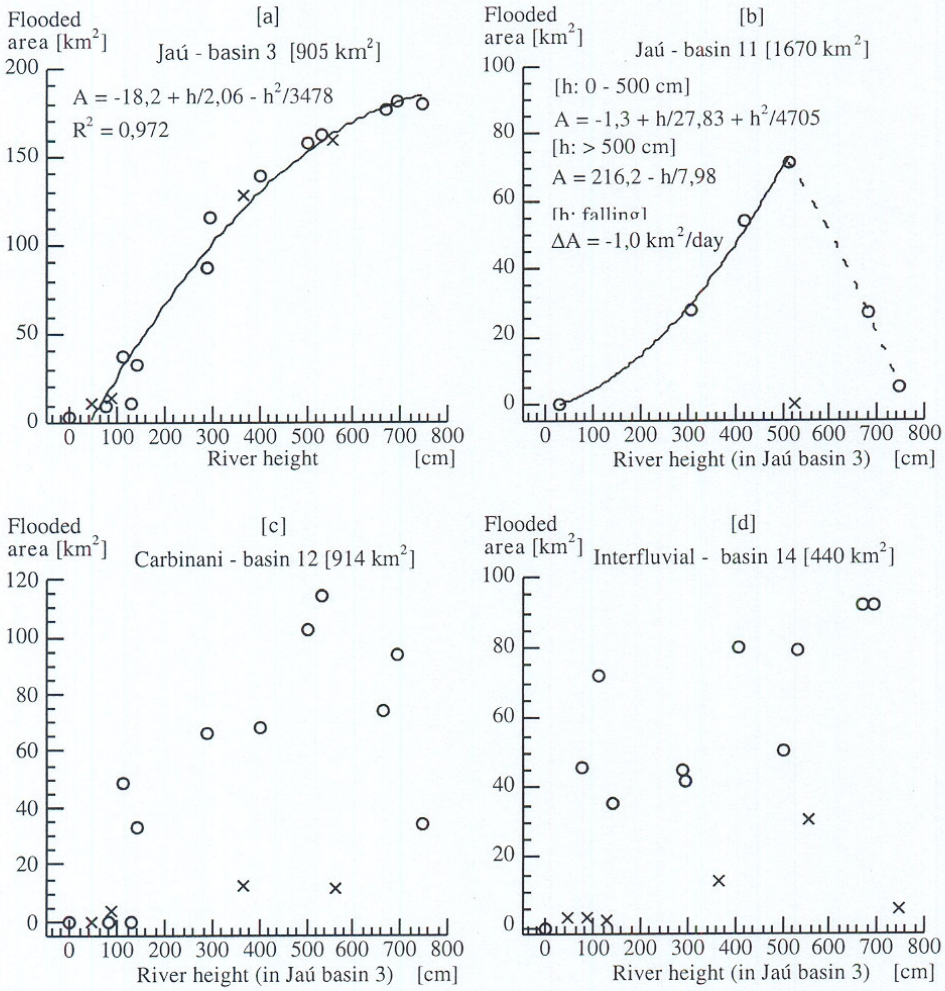

Figure 6. *River stage height vs. flooded area for four sub-basins in the Jaú river basin (O - rising stages; X - falling stages). Analytical relationships between river stage and flooded area could only be obtained for sub-basins along the Jaú main channel (1-11)*

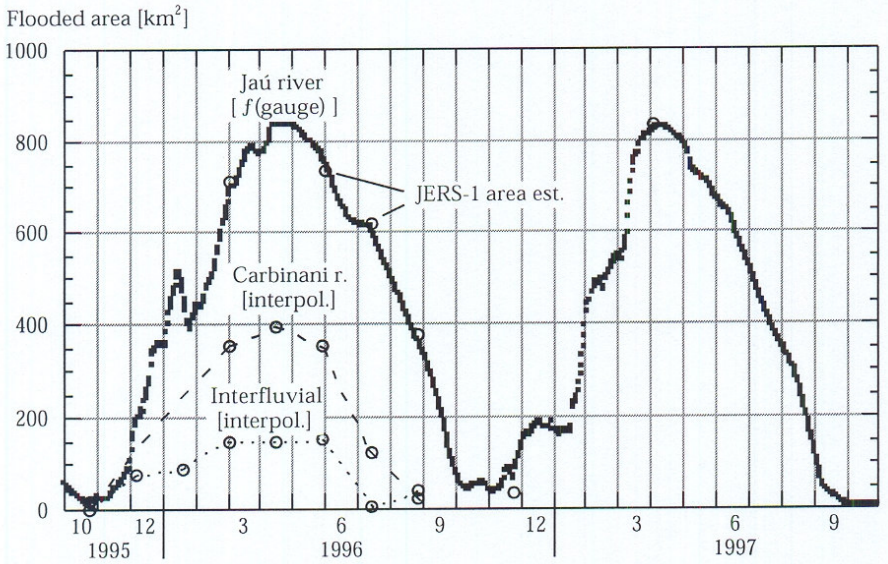

Figure 7. Variations in flooded area during the 95/95 and 96/97 flood cycles. Area estimates in the Jaú river (basins 1-11) derived analytically from daily gauge records. Estimates for the Carbinani river and the interfluvial area derived by linear interpolation between estimates in JERS-1 SAR data.

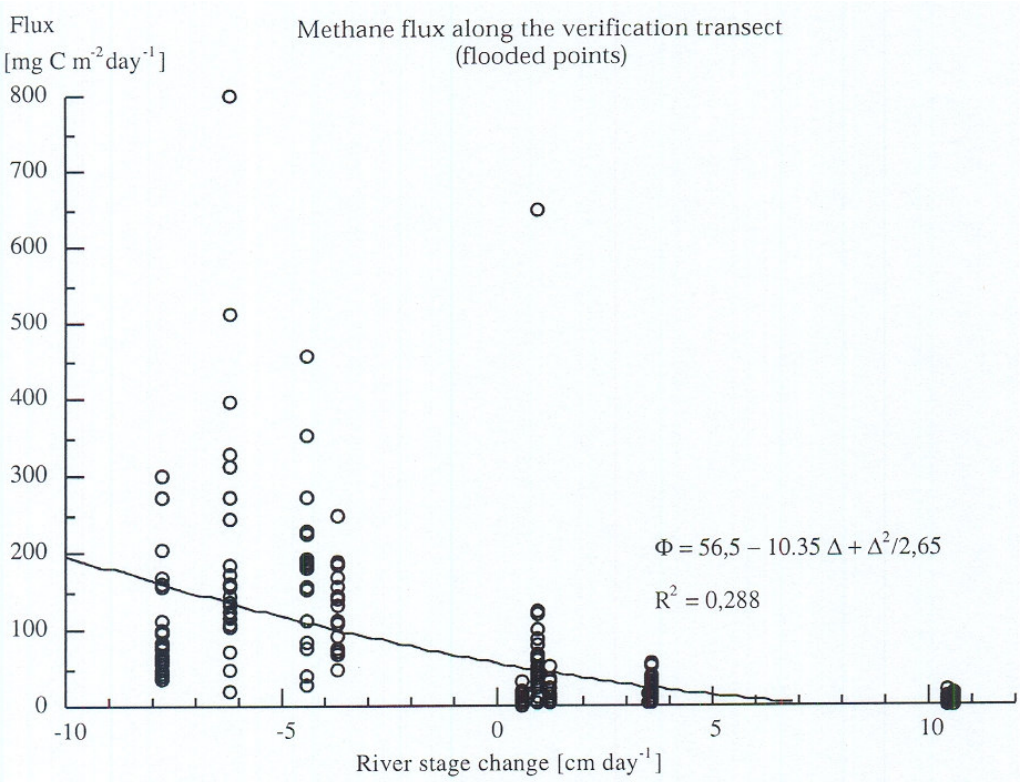

Figure 8. *Empirical relationship linking methane fluxes to daily rate of change in river stage.*

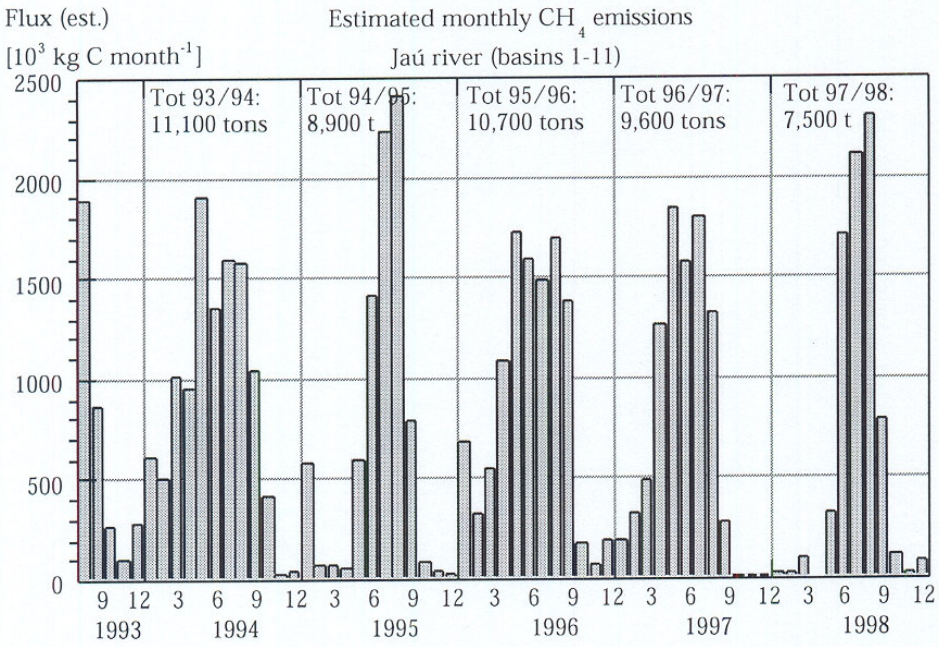

Figure 9a. *Estimated monthly CH_4 emissions (10^3 kg of C month^{-1}) from the Jaú river (basins 1-11) 1993-1998. Accumulated annual estimates are given for each flooding cycle.*

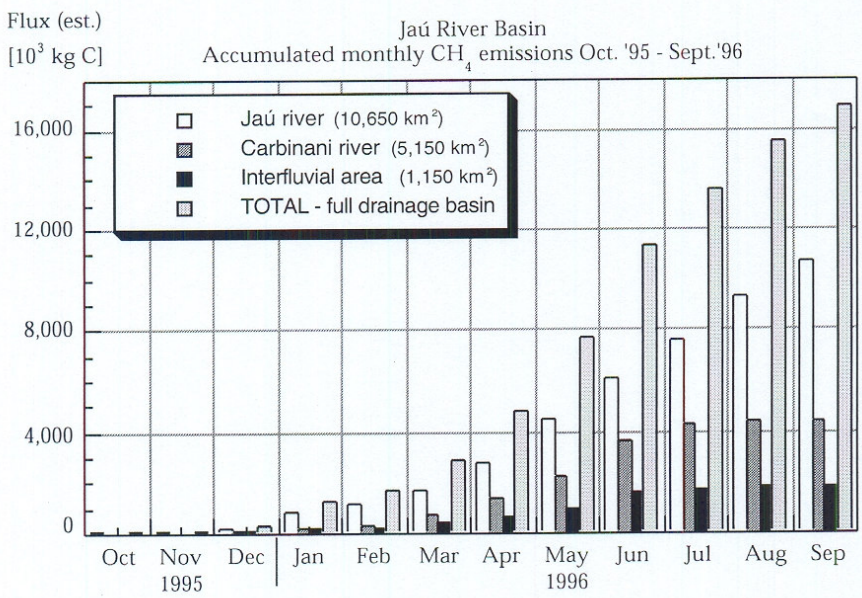

Figure 9b. *Accumulated monthly CH_4 emissions during the 1995/1996 flooding cycle for the entire Jaú river basin. Flood estimates in for the Carbinani and interfluvial area obtained through linear interpolation between JERS-1 derived area estimates.*

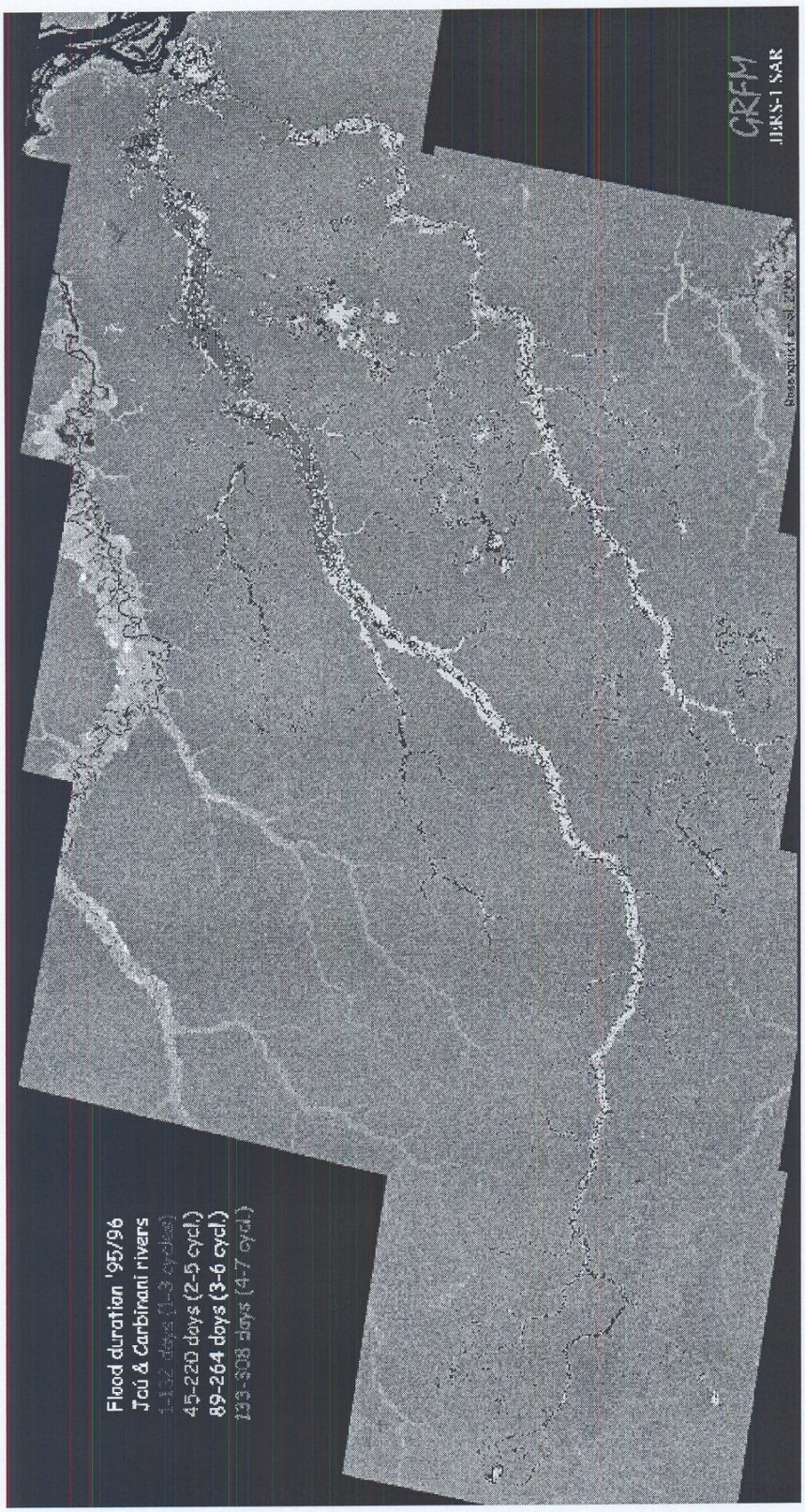

Figure 10. Flood duration in the Jaú river drainage basin, extracted from JERS-1 SAR time sequence of 5 data takes during the 1995-1996 flood cycle. Original pixel spacing 100 metres. GRFM © NASDA/MITI/JRC

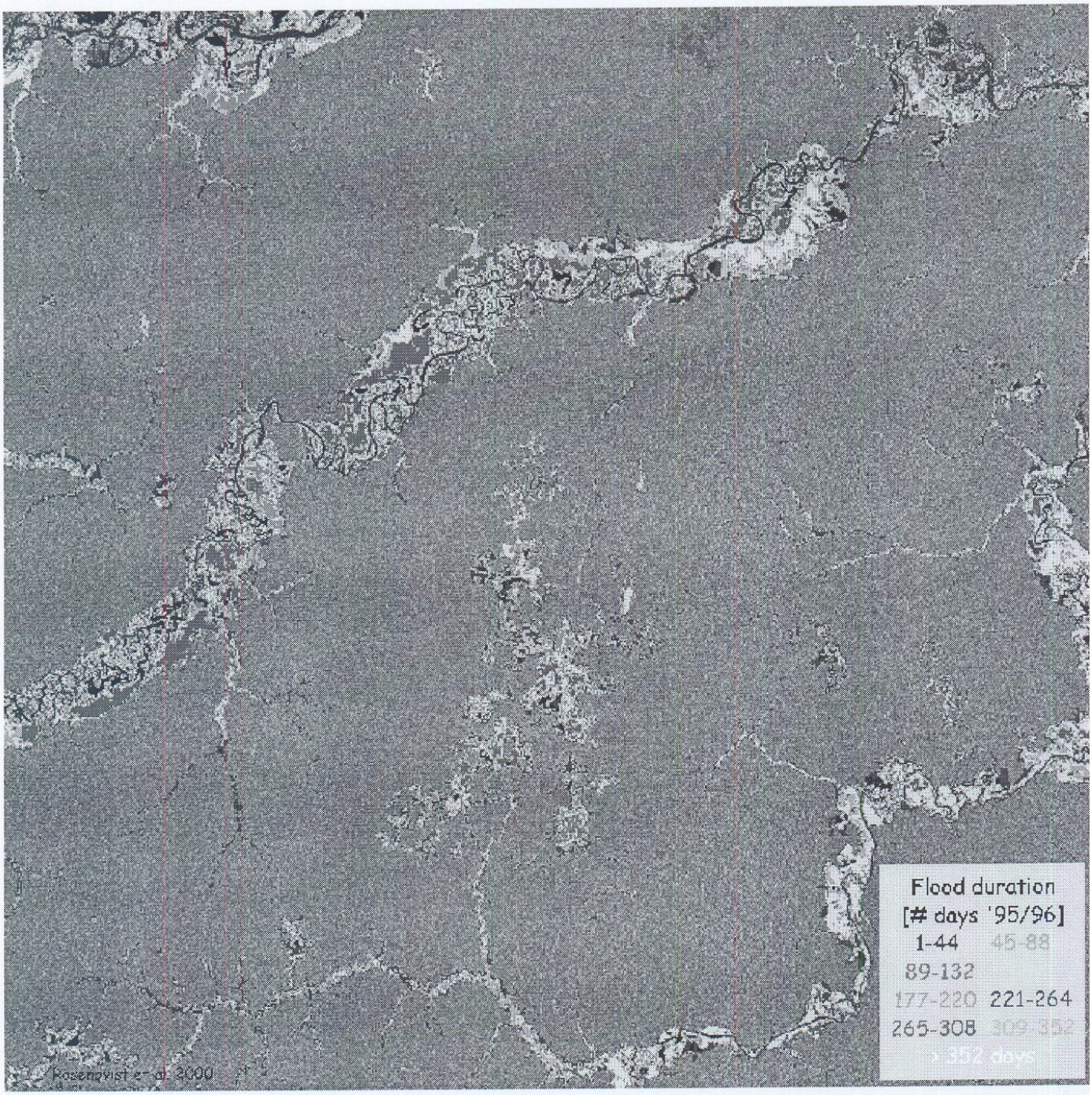

Figure 11. The Jaú and Carbinani rivers, and the rain fed interfluvial area (JERS path 418). Flood duration map extracted from JERS-1 SAR time sequence of 9 consecutive data takes. Temporal resolution 44 days. GRFM © NASDA/MITI

Transect [km]	3-MAR 1996	30-MAY 1996	13-JUL 1996	26-AUG 1996	22-NOV 1996	18-FEB 1997	3-APR 1997
0.1	1511	1644	1473	1747	(1396)	1639	1836
0.2	1641	1628	1569	1507	1320	1532	1646
0.3	1787	1527	1451	1535	1189	1403	1498
0.4	1422	1538	1365	1445	1154	1195	1408
0.5	1321	1483	1444	1544	1184	1427	1493
0.6	1436	1372	1483	1393	1043	1356	1535
0.7	1518	1657	1408	1417	1117	1316	1446
0.8	1597	1556	1524	1374	1104	1412	1387
0.9	1632	1405	1569	1660	1281	1235	1637
1.0	1641	1610	1293	1569	1205	1478	1581
1.1	1476	1335	1485	1410	1023	(1340)	1715
1.2	1571	1320	1305	1459	1023	(1296)	1490
1.3	1397	1514	1401	1498	1081	(1319)	1522
1.4	(1494)	1398	1323	1548	1129	(1256)	1692
1.5	(1585)	1519	1481	1608	1215	(1131)	1805
1.6	(1273)	1521	1548	1607	1126	(1118)	1864
1.7	(1401)	1324	1448	(1446)	1005	1026	(1653)
1.8	(1232)	1746	1638	(1349)	1068	1164	(1570)
1.9	(1168)	1550	1455	(1516)	1253	1167	(1517)
2.0	1073	(1635)	1400	(1328)	1209	1167	(1425)
2.1	1182	(1455)	1624	(1319)	1129	1149	(1232)
2.2	1219	(1276)	1498	(1252)	1009	1400	(1198)
2.3	1129	(1302)	(1436)	1253	1222	1290	1215
2.4	1139	(1243)	(1270)	1241	1269	1107	992
2.5	1103	(959)	(1085)	1017	1190	991	1123
2.6	1173	1061	(1185)	1015	1072	920	1028
2.7	1196	1053	1073	1100	933	1174	1071
Stage	409 cm	667 cm	747 cm	555 cm	77 cm	291 cm	503 cm

Table I. *Temporal variations in L-band backscatter (linear DN) along the Jaú transect. Shaded and white boxes indicate in-situ verified flooded resp. dry points. Figures within brackets indicate points with unverified or mixed flooding conditions.*

	Flooded igapó	Dry igapó	Terra firme	Dry igapó + Terra firme
n	288	174	96	270
Mean [DN]	1504.9	1135.5	1109.6	1126.6
Mean [dB]	-4.65	-7.10	-7.30	-7.16
Std Dev.	137.2	97.6	94.6	97.2
Min	1195	920	939	920
Median	1499	1131	1089	1115
Max	1948	1403	1475	1475

Table II. *L-band backscatter statistics (linear DN) of in-situ verified points along the transect.*

Jaú river (basin 3) A_{TOT}: 905.2 km^2															
Threshold		Flooded area [km^2] Uncorrected estimates (A'_F)						Correction coeff.		Flooded area [km^2] Corrected estimates (A_F)					
DN	[dB]	95-10	96-03	96-05	96-07	96-08	96-11	ε_{DRY}	ε_{FLOOD}	95-10	96-03	96-05	96-07	96-08	96-11
1270	-6.12	89.3	206.1	242.0	244.2	223.3	97.1	0.097	0.035	1.7	136.3	177.6	180.2	156.1	10.7
1280	-6.06	76.0	193.7	229.2	231.6	210.0	83.4	0.074	0.035	10.1	142.2	182.0	184.7	160.5	18.4
1290	-5.99	63.8	182.8	217.9	220.0	198.9	72.6	0.063	0.038	7.5	139.9	179.0	181.3	157.8	17.4
1300	-5.92	53.7	173.1	207.6	209.4	189.1	62.0	0.052	0.052	7.4	140.6	179.2	181.2	158.5	16.7
1310	-5.85	45.5	164.7	198.2	200.5	180.5	53.0	0.048	0.069	2.4	137.3	175.3	177.8	155.2	10.8
1320	-5.79	38.2	157.0	190.4	192.6	173.2	45.6	0.037	0.083	5.3	140.4	178.2	180.8	158.8	13.8
1330	-5.72	32.6	150.2	183.1	185.6	166.7	39.0	0.033	0.097	3.1	138.3	176.1	179.0	157.2	10.5
Mean A'_F [km^2]		57.0	175.4	209.8	212.0	191.7	64.7	Mean A_F [km^2]		**5.4**	**139.3**	**178.2**	**180.7**	**157.7**	**14.0**
St.dev.		20.57	20.12	21.25	21.20	20.35	20.93	St.dev.		**3.14**	**2.07**	**2.22**	**2.16**	**1.77**	**3.42**

Table III. *Flood area estimates in Jaú river (basin 3) before and after correction of misclassified pixels. The correction coefficients (ε_x) indicate the fractions of misclassified pixels for a given threshold value prior to correction.*

Transect [km]	9-OCT-1996	20-NOV-1996	11-JAN-1997	23-FEB-1997	29-MAR-1997	26-MAY-1997	29-JUN-1997	13-AUG-1997	27-SEP-1997	9-NOV-1997	21-DEC-1997	4-MAR-1998	9-APR-1998	8-MAY-1998	25-JUN-1998	16-JUL-1998	16-AUG-1998	15-SEP-1998
0	-1.9	-0.8	-11.6	12.0	25.2	4.0	110.6	351.4	4.9	-0.6	-4.0	-0.5	-1.1	3.8	-11.7	69.4	64.0	4.4
0.3	-1.1	-1.2	17.7	29.2	25.2	9.4	144.7	118.5	2.4	-0.6	-2.2	-0.5	-0.9	6.0	14.8	39.7	153.8	0.9
0.6	47.2	-0.5	-0.9	21.3	22.1	4.5	108.0	273.0	2.3	0.3	2.4	-0.7	-1.4	3.1	23.6	41.2	76.6	1.4
0.9	-0.7	-0.2	-0.4	6.1	10.7	8.6	148.7	105.5	1.1	1.9	-0.9	-0.9	0.1	2.1	28.0	46.7	65.5	0.9
1.2	2.3	-0.5	-0.5	17.4	20.4	9.3	118.6	84.4	0.8	-0.9	2.7	-0.7	-1.2	-0.5	29.2	34.3	72.0	1.3
1.5	4.5	-0.8	-0.1	-0.8	14.3	14.1	170.1	166.8	2.6	-0.3	-4.1	-0.7	-0.6	-1.6	22.2	71.0	169.7	1.1
1.8	0.6	-1.0	-0.5	-0.8	10.3	20.0	152.7	1573.3	28.1	-0.3	-0.6	-0.3	-0.8	-0.3	18.2	190.6	82.0	0.5
2.1	-0.4	-0.6	-0.4	-0.9	0.1	15.6	149.2	2.8	0.7	-0.5	0.5	-1.0	-0.8	-0.3	9.3	31.9	80.9	0.9
2.4	-1.1	0.0	-0.4	-0.1	-0.6	33.9	258.3	0.8	-1.0	-0.8	3.1	-3.0	-1.0	-0.7	-43.0	5.1	-2.6	0.1
2.7	-0.3	-0.5	-0.5	0.7	-0.4	-1.4	6.0	0.8	-1.5	-1.0	2.5	-0.4	-0.7	-1.0	-2.4	0.0	-0.4	-1.3

Table IV. *Temporal variations in CH_4 flux [mgC/m^2/day] along the 10 transect points.* ***Shaded boxes*** *indicate inundated points.*

	1995		1996						
Jaú basin	22-26 Oct			2-6 Mar		29 May-6 Jun	12-16 Jul	25-29 Aug	
Transect path	23 Oct	6 Dec	19 Jan	3 Mar	16 Apr	30 May	13 Jul	26 Aug	9 Oct

Table V. *JERS-1 SAR data availability over the Jaú river drainage basin (paths 417-421) and the verification transect (path 418), respectively, during the 1995/1996 flood cycle.*